ACS OMEGA

Open Access

http://pubs.acs.org/journal/acsodf

Article

Comprehensive Analysis of Connectivity and Permeability of a Pore-Fracture Structure in Low Permeability Seam of Huainan−Huaibei Coalfield

Zhangfei Wang, Huihuang Fang,* Shuxun Sang,* Jinran Guo, Shua Yu, Huihu Liu, and Hongjie Xu

Cite This: *ACS Omega* 2024, 9, 15357−15371

Read Online

ACCESS | Metrics & More | Article Recommendations

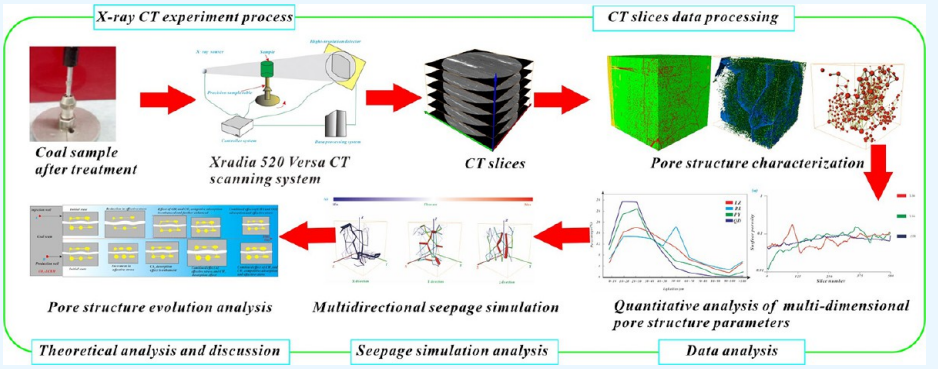

ABSTRACT: The connectivity and permeability of the coal seam pore structures control the occurrence and migration of coalbed methane. Coal samples were used from Huainan−Huaibei to reconstruct three-dimensional models of the pores and an equivalent pore network model, Statistical pore structure characteristic parameters. The pore structure of the coal reservoir was analyzed from the direction of multidimensional and multiangle. It shows that based on quantitative analysis, the representative Elementary volume of 500 × 500 × 500 was the most suitable experimental volume. The *Y*-axis direction of the Renlou sample had poor pore connectivity compared to that of other samples. Large volume connected pores dominated their pore systems. In terms of coal sample pore connectivity, the coal samples from the Liuzhuang and Qidong regions had pore connectivity better than those from the other regions. The pore connectivity of the Liuzhuang coal samples was the best. In terms of coal permeability, the Liuzhuang sample had better permeability than the other three samples, and the permeability was the best in the *Y*-axis direction. For all the combinations of the different types of throats, the shorter the throat, the greater the equivalent radius and the better the permeability. Conversely, the worse the permeability. During gas injection production, the closer the gas injection area was to the gas injection well, the poorer the connectivity and the lower the permeability over time. Near the production area, where the CO_2 did not reach the production area, the fracture porosity and effective connected porosity of the coal reservoir increased over time. When CO_2 reached the production area, the change in its connected pore structure was consistent with the change in the connected pores in the gas injection area. With this study, the coal seam pore structure on a microscale was characterized. A comprehensive analysis of the coal reservoir pore connectivity and permeability was completed. The study results are significant for the exploration and development of coalbed methane in the Huainan−Huaibei coalfield.

1. INTRODUCTION

Coal is a complex porous medium, that not only contains solid components, but also a large number of pores and fractures.[1,2] The distribution of the pore and fracture structure of coal stores coalbed methane and allows for its migration. It also directly affects the accumulation and migration of fluids and plays a very important role in the exploration and development of coalbed methane.[3,4] The pores and fractures not only restrict the gas content of the coal seam but also affect the economic viability of the coal seam.[5] Therefore, whether it is direct coalbed methane extraction or gas injection extraction (CO_2-ECBM), the connectivity of the pore and fracture system has always been the main aspect affecting the efficiency of CO_2 injection and CH_4 production.[6] The analysis of the core parameters of pores and fractures is the key to studying the connectivity and

Received: December 21, 2023
Revised: February 18, 2024
Accepted: March 1, 2024
Published: March 20, 2024

permeability of coal reservoirs as the structural characteristics of pores and fractures are geometrical and topological.[7,8] The comprehensive analysis of pores and fractures in our study not only assists in evaluating the connectivity and permeability of the coal reservoirs but also provides a theoretical basis for coalbed methane mining and further affects the engineering of CO_2-ECBM technology.

The main current research methods for coal reservoir pores and fractures include the traditional low-temperature liquid nitrogen method and mercury injection method,[9,10] high-resolution scanning electron microscopy,[11,12] CT scanning,[13] nuclear magnetic resonance, other photo electromagnetic observation methods[14,15] and X-ray microcomputed tomography (CT). CT is a widely used nondestructive testing method for analyzing the pore and fracture structure of reducing coal.[16−18] Previous scholars have used CT technology to analyze different aspects of the coal reservoir pore and fracture structure. Analyses include (1) extracting pore and fracture structure, and conducting qualitative and quantitative characterization;[19−21] (2) statistical analysis of pore volume fraction and several different diameters;[22−24] (3) studying the evolution of pore and fissure structure influenced by different factors;[25−27] and (4) studying the influence of pore fracture structure characteristics on permeability and seepage simulation.[28−30] For this study, coal rock was divided into two parts: pores and solids. The pore structure of the coal reservoir was analyzed from multiple dimensions and angles.

The geometric structure features that were determined using the pore structure level mainly refer to the geometric size and shape distribution of pores and throats. The core parameters include the pore radius, the throat radius, the throat length, and the pore volume.[31] The topological structure features mainly refer to the correlation features between the pores and throats, while the core parameters include the coordination number and the connectivity function.[32] The quantitative analysis of pore structure parameters is helpful in understanding the pore connectivity and permeability of coal reservoirs. At the same time, combined with the three-dimensional visualization model of pore structure and the equivalent pore network model, the multidimensional and multiangle detailed analysis of the pore structure of a coal reservoir can be realized.

Coal samples from the Liuzhuang, Renlou, Panyi, and Qidong areas in the Huainan−Huaibei region were selected for this study, and CT technology scans were used to obtain thin-section images of the CT scans. The 3D visualization AVIZO software was used to process thin section images and to construct a 3D pore model and an equivalent pore network model of the coal samples. Different algorithms and the Representative Elementary Volume (REV) were used to analyze the pore structure in the coal from a multidimensional multiangle perspective. First, the surface porosity was analyzed from a two-dimensional perspective to understand the changes in surface porosity in different directions. Second, the pores were extracted and classified into connected and isolated pores to obtain the volume proportion and distribution of the connected and isolated pores. Finally, an equivalent network model was built based on the connected pores to obtain the pore parameters, the throat parameters, and the coordination numbers. Third, the local Angle and the overall Angle of the sample were used to analyze the sample connectivity using the pore structure parameters. Lastly, the permeability of the coal sample in different directions was simulated by using the equivalent pore network model, and based on the results, discussed the evolution of the pore structure in the coal reservoir during the gas injection production (CO_2-ECBM).

The innovation of this research is mainly reflected in the following aspects: (1) pore structure, connected pore structure, and isolated pore structure of the coal reservoir are visually reconstructed to build the equivalent pore network model. (2) The pore structure analysis from a multidimensional perspective was completed by using a variety of algorithms and combining representative elementary volume (REV). (3) The pore connectivity analysis of the coal samples was completed by using coordination parameters with the constructed equivalent pore network model. (4) The permeability experimental analysis of the pore structure in different directions of the coal samples was analyzed by using the equivalent pore network model. Lastly, a permeability analysis of the pore structure of the coal samples was proposed by using the combination and collocation of the different types of throats. This study can provide a theoretical basis for the exploration and development of the CBM in the Huainan−Huaibei coalfield and can enrich the development of digital core technology.

2. MATERIALS AND PREPARATION

2.1. Coal Sample Preparation. Coal samples were obtained from the coal mines of the Liuzhuang, Renlou, Panyi, and Qidong in the Huainan−Huaibei areas, with sample numbers LZ, RL, PY, and QD respectively (Figure 1). The

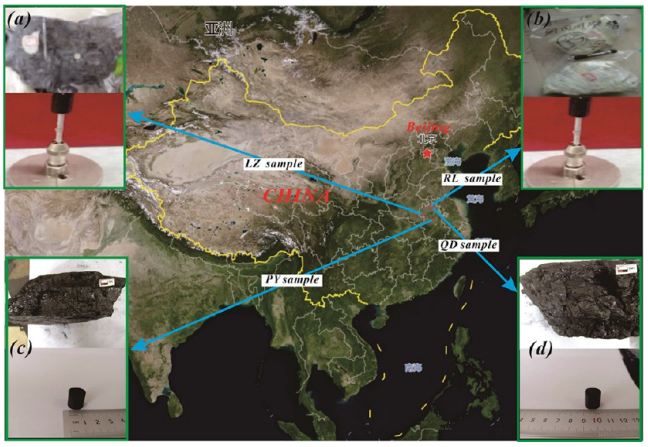

Figure 1. Test sample sampling point distribution. The map of China was downloaded from Amap, and other photos were taken by Zhangfei Wang. (a) LZ, (b) RL, (c) PY, and (d) QD.

coal of the LZ coal mine is medium ash, low to extra low sulfur, low to extra low phosphorus, high calorific value, and high-quality gas coal. The coal of the RL coal mine is a high-quality gas coal. The PY coal mine has coal of excellent quality, with "three low and one high," that is, low ash, low sulfur, low phosphorus, and high caloric content coal. It is an excellent coking and thermal coal. The QD coal contains gas coal, fertilizer coal, and 1/3 coking coal that contains a small amount of anthracite. The coal samples were collected from fresh underground working faces and packaged and transported under relevant national and international standards (GB/T 6948-2008 and GB/T 8899-2013). The collected samples were also wrapped with toilet paper and plastic wrap to prevent water exposure and oxidation.

2.2. CT Experiment. X-ray micron CT uses conical X-rays to penetrate the object, magnify the image through the objective

https://doi.org/10.1021/acsomega.3c10247
ACS Omega 2024, 9, 15357−15371

lens, and reconstruct a 3D stereo model through a large number of X-ray attenuation images obtained via a 360° rotation of the precision sample table. The pore structure and relative density of the core can be obtained without damaging the sample via the attenuation information on the X-ray energy during penetration of the object. In this experiment, the X-ray CT used the Xradia 520 Versa CT scanning system produced by Carl Zeiss of Germany (Figure 2). This system consists of an X-ray source, a

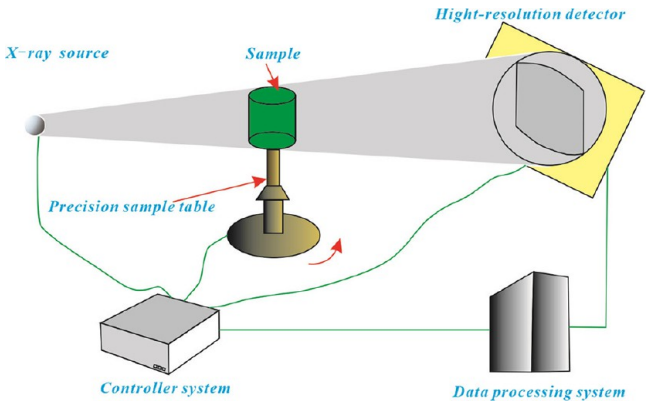

Figure 2. Schematic diagram of a CT scan.

precision sample table, a high-resolution detector, a data processing system, and a controller system. It can meet the requirements of high-precision nondestructive testing of small-diameter samples.

To allow for further sample preparation and scanning work, the collected fresh coal samples were prepared into cylinders of certain specifications according to the requirements of the scanning experiment for the testing unit. After an X-ray CT scan, some parameters can be obtained from the four tested samples (Table 1).

Table 1. Dimensions of Two Coal Samples Used in This Study

sample ID	sample shape	number of voxels	voxel size
LZ	cylindrical type	2500 × 2500 × 1900	10.00 μm
RL	cylindrical type	1810 × 1801 × 2001	8.02 μm
PY	cylindrical type	2400 × 2400 × 1972	8.45 μm
QD	cylindrical type	1060 × 1019 × 2429	3.00 μm

2.3. 3D Visualization Reconstruction of CT Images. The scanned CT thin sections can be used to develop the 3D visualization model of the segmentation and combination of the coal matrix, pores, and minerals. The main steps include noise reduction processing, threshold selection, image segmentation, and performing representative volume unit analysis, pore analysis, and equivalent pore network model reconstruction (Figure 3). A median filter noise reduction can ensure the integrity of the pores and allow for the transition between the pores and the matrix so that the pores can be distinguished from other components.[33] The watershed algorithm can be used for threshold selection of the pore, matrix, and mineral phases,[34] The threshold selection is done via the Interactive Thresholding operation of the AVIZO software. The representative elementary volume (REV) is a basic method used to quantify the scale effect. When the coal size is larger than the REV scale, its physical and mechanical characteristic parameters are usually stable.[35] At this time, the characteristics of the coal body for the REV size represent the characteristics of the entire coal body. This reduces the computer calculation time and improves the accuracy of the experimental data.

A 1000 consecutive CT sections in the middle of the coal sample were performed for this study. Different pixel sizes were cut according to different conditions for the CT sections of the coal sample itself. The watershed algorithm was used to select the threshold value. After the threshold value was selected, the slices that were processed by the threshold value were compared to the original two-dimensional slices to detect whether some pores should be deleted. At this time, partial fine-tuning of the image segmentation threshold is carried out. For the selection of REV, a 500 × 500 × 500 voxel square should be selected and extracted from the middle of the coal sample. Finally, via the segmentation and combination of the coal matrix, the pores and minerals can be visualized through the functional operation of segmentation by AVIZO software (Figure 4), to achieve a three-dimensional reconstruction of CT images. The AVIZO software PNM model (pore network model) was used to construct the equivalent pore network model and complete the corresponding analysis.

2.4. Pore Structure Characteristic Parameters. For this study, the coal rock was divided into pore and solid parts. Since two-dimensional slices were used to develop a three-dimensional reconstruction of pores through the AVIZO software for this experiment, the connectivity of the different dimensions of the coal and rock pores can be studied from both two- and three-dimensional perspectives. The two-dimensional angle parameters mainly consider the surface porosity, while the three-dimensional Angle parameters mainly consider the pore volume, throat parameters, and coordination number.

2.4.1. Surface Porosity. The two-dimensional thin-section images that were obtained by the CT scan are displayed in the form of pixels and show both including the pore area, the coal matrix area, and the mineralized area. In this study, the pore and solid areas (Figure 5) were considered. The surface porosity is the ratio of the pore area to the overall area in the picture (eq 1). The study of the surface porosity of the sample helps us understand the change in the local pore structure of the coal.[36]

$$\theta = \frac{S_{\text{pore}}}{S_{\text{pore}} + S_{\text{solid}}} \tag{1}$$

where θ is the surface porosity; S_{pore} is the pore area; and S_{solid} is the solid area.

2.4.2. Pore Volume. The pores in the coal seam serve as the storage, migration, and production place of coalbed gas. Therefore, the volume and distribution of the coal seam pores affect the exploration and development of the coalbed gas. Using the maximum-sphere algorithm, each pore position is assumed to be a sphere equal to its volume, and the equivalent pore size can, therefore, be obtained by eq 2.[37]

$$D_{\text{eq}} = \sqrt[3]{6V_{\text{pore}}/\pi} \tag{2}$$

where, D_{eq} is the equivalent pore size, micron; V_{pore} is a single pore fracture volume (micron cubic).

2.4.3. Throat Parameter. The throat is the channel that connects the pores and serves as the main channel through which fluid flows from one pore to another. The throat parameters mainly focus on the length and radius of the throat. The length of the throat is the path of fluid migration, and the longer the connectivity, the worse fluid migration will be. The

https://doi.org/10.1021/acsomega.3c10247
ACS Omega 2024, 9, 15357−15371

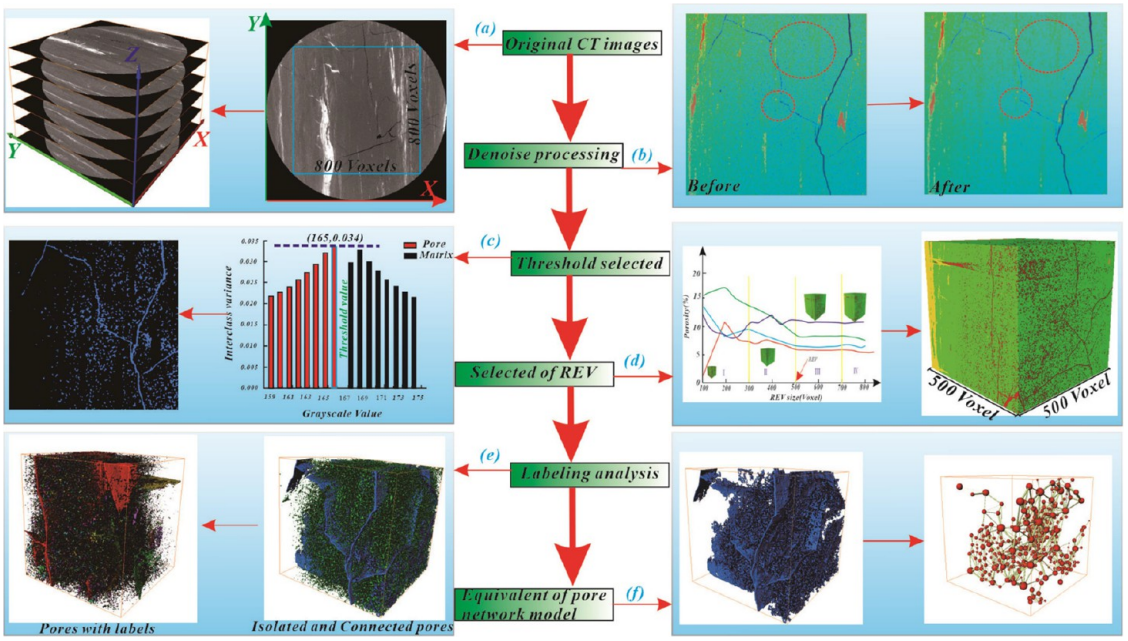

Figure 3. Schematic diagram of extraction process of the pore model with labels. (a) Original CT images; (b) denoise processing; (c) threshold selected; (d) selected REV; (e) labeling analysis; (f) equivalent of the pore network model. The photographs were taken by Zhangfei Wang.

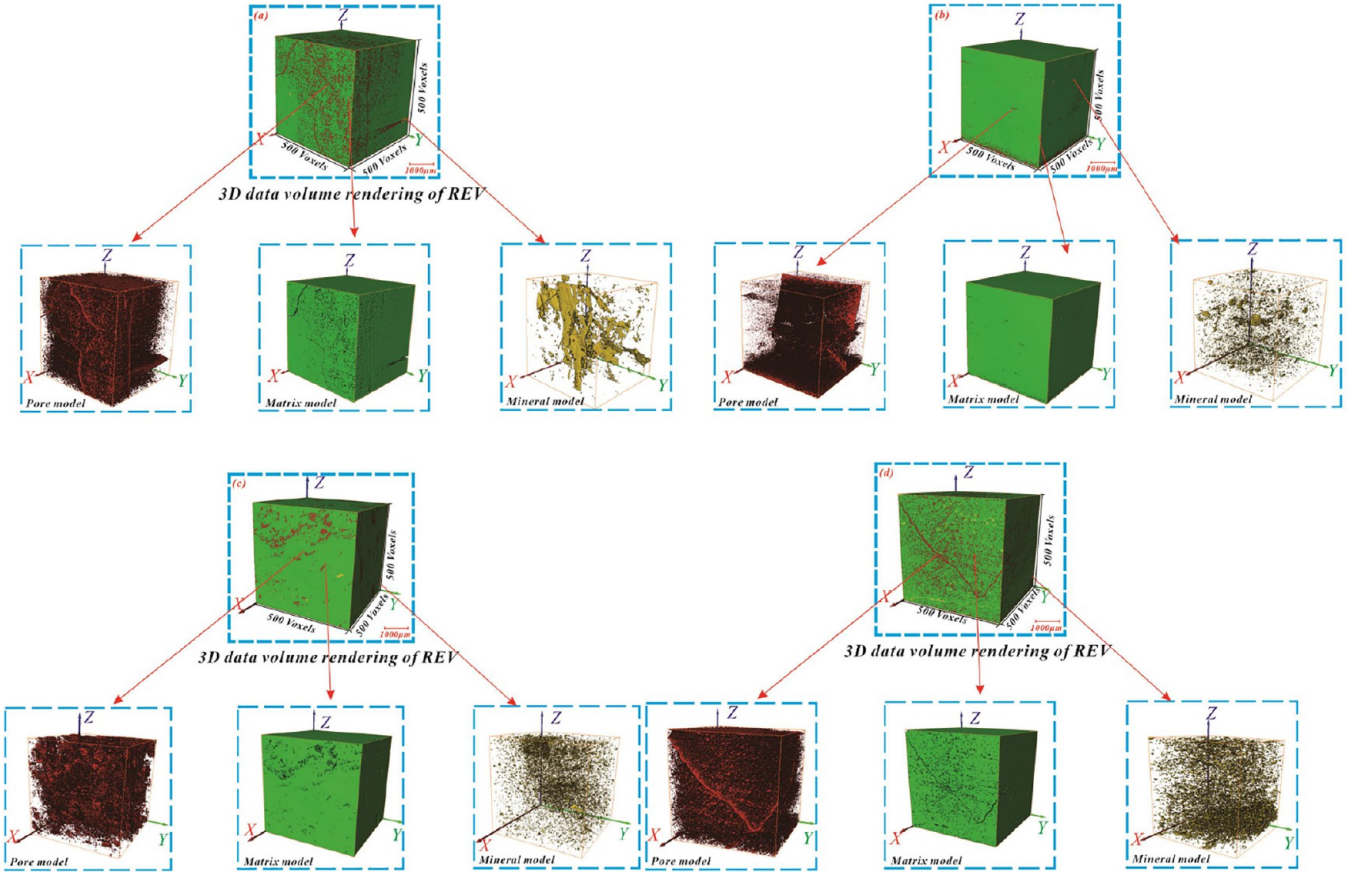

Figure 4. 3D visualization reconstruction of the coal sample. (a) LZ sample; (b) RL sample; (c) PY sample; and (d) QD sample.

throat radius is the width of the throat through the channel, and the larger the throat radius is, the better the connectivity.

2.4.4. Coordination Number. The coordination number refers to the number of throats connected to each pore.[38,39] The size of the coordination number controls the flow and production of fluid in the pore. The larger the coordination number, the better the connectivity of the pore. When the coordination number is 1, the pores do not have connectivity and are called dead-end pores (Figure 6).

https://doi.org/10.1021/acsomega.3c10247
ACS Omega 2024, 9, 15357−15371

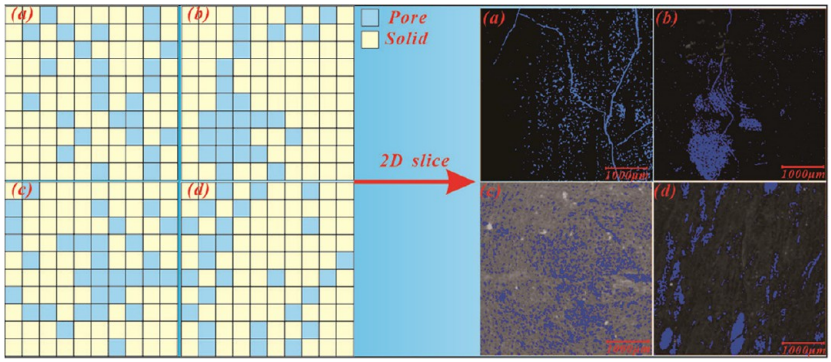

Figure 5. 2D slice pixel map: (a) LZ sample; (b) RL sample; (c) PY sample; and (d) QD sample.

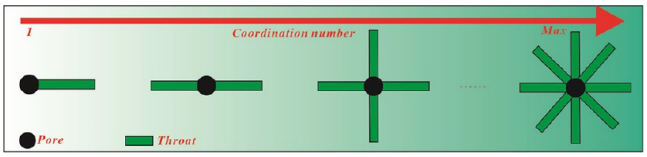

Figure 6. Coordination number diagram.

2.4.5. Principle of Reservoir Permeability Model. The coal reservoir permeability simulation in this study is based on the equivalent pore network model. This model is combined with the built-in AVIZO software algorithm to simulate and analyze the absolute permeability in three different directions: *X*, *Y*, and *Z*. The absolute permeability simulation principle of the software is as follows:

Absolute permeability: Flow is laminar in all directions (Poiseuille flow).

To calculate the absolute permeability of the model, the network is assumed to be filled with only one phase. During steady-state flow of an incompressible fluid, the mass conservation for each pore body is described as (eq 2):

$$\sum_{i \to j} q_{ij} = 0 \tag{3}$$

where the summation is performed on all of the pore j connected to the pore i; q_{ij} represents the flow rate between pore i and pore j.

Under laminar flow conditions, the relation between the pressure drop and flow rate is linear (eq 3):

$$q_{ij} = g_{ij}(P_i - P_j) \tag{4}$$

where g_{ij} represents the conductance of the throat between pore i and pore j. Since the conducting throats are represented by cylindrical pipes of radius r_{ij} and length l_{ij}, the hydraulic

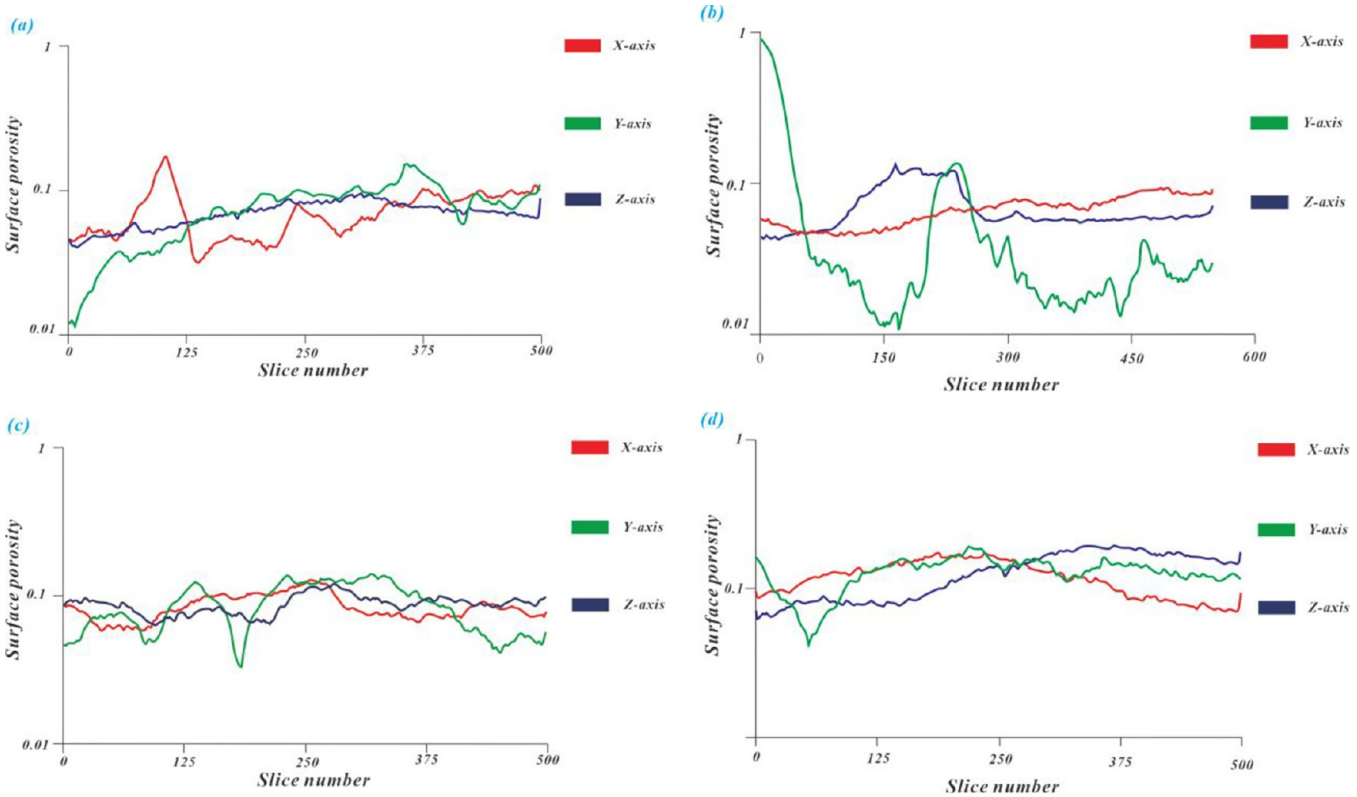

Figure 7. Surface porosity for the three-dimensional pore structures. (a) LZ sample; (b) RL sample; (c) PY sample; and (d) QD sample.

https://doi.org/10.1021/acsomega.3c10247
ACS Omega 2024, 9, 15357−15371

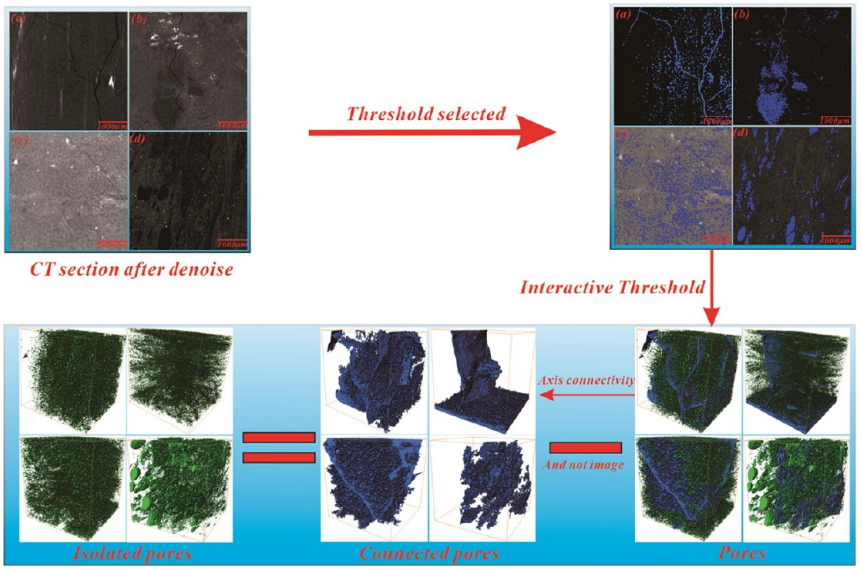

Figure 8. 3D pore structure extraction process: (a) LZ sample; (b) RL sample; (c) PY sample; and (d) QD sample.

conductance is given by Poisuille's law, where μ is the fluid viscosity (eq 4):

$$g_{i,j} = \frac{\pi}{8\mu}\frac{r_{ij}^4}{l_{ij}} \tag{5}$$

The pressure difference that is imposed across the network results in a linear system of equations that is solved numerically (eqs 3 and 4). This leads to the following matrix equation: $G^*P = S$, where G is the matrix of conductance, which is a symmetrical matrix of dimensions N^*N, where N is the number of pores in the network. P is a vector of the size N corresponding to the pressure in each pore. S is a vector of size N, which is constrained by the pressure boundary conditions at the inlet and outlet of the system. The total flow rate can then be computed: $Q = \sum (P_i - P_j)g_{ij}$ on each pair of pores i, j intersecting an arbitrary cross-section of surface A. The permeability (k) of the network is then finally deduced from Darcy's law (eq 5):

$$k = \frac{Q}{\Delta P}\frac{\mu L}{A} \tag{6}$$

where $\triangle P$ is the gradient of pressure applied to the boundary (input pressure − output pressure) and L is the length of the network in the flow direction.

3. RESULTS

3.1. 2D Slice Pore Analysis. The information contained in the two-dimensional thin section image includes the coal matrix area, pore area, and mineralized area. The change in the local pore structure of the coal can be understood through a study of its surface porosity. If the surface porosity is 0 or close to 0, it means that the pores in this part are not connected or have poor connectivity.

Based on Figure 7, the surface porosity changes in different directions, the porosity of coal samples in the Y-axis direction in the Huainan−Huaibei area is complex, and the porosity of LZ and RL coal samples in the Y-axis direction is close to 0, which means that the connectivity of the coal samples in the Y-axis direction is poor. The variation in the amplitude of the porosity for coal samples from PY and QD of the two places on the Y-axis is large, indicating that the pore structures of these two places in the Y-axis direction are relatively complex. Therefore, it can be seen that the pore development of coal samples in the Huainan−Huaibei area based on the Y-axis direction is relatively complex. At the same time, based on Figure 7, it can be seen that the value of surface porosity in different directions in the Huainan−Huaibei area basically fluctuates around 0.1%, reflecting the low permeability characteristics of coal samples in the Huainan−Huaibei area.

3.2. Characterization and Analysis of the Pore Structure. *3.2.1. 3D Pore Structure Reconstruction.* The pore structure of the coal samples includes two types of connected and isolated pores. Therefore, these two types of pores were extracted and reconstructed separately in this study. After image segmentation and visualization, the coal matrix, pores, and minerals were extracted separately to visualize the separation of the pores and solid parts. The axis connectivity algorithm of the AVIZO software can be used to extract the structure of connected pores after the pore structure is obtained. The isolated pores can be extracted from the total by excluding the connected pores using the image algorithm (Figure 8).

3.2.2. Quantitative Analysis of the Pore Structure. Isolated pores generally store coalbed methane, while connected pores generally serve as the migration and production channels of coalbed methane. It is therefore very important to perform a quantitative analysis of the two kinds of pores during the exploration and development of coalbed methane. Statistical data can be used to divide the isolated pores into three types: A, B, and C. The type A pore has a volume of less than 10^4 μm^3. The type B pore has a volume of 10^4−10^5 μm^3; while the type C pore are pores larger than 10^5 μm^3 in volume. Table 2 shows the

Table 2. Volume Percentage of Isolated Pores

sample number	percentage of total isolated pore volume (%)	percentage of pore volume (%)		
		A	B	C
LZ	3.00	0.18	0.96	1.86
RL	1.32	0.34	0.01	0.97
PY	4.99	0.08	0.36	4.55
QD	3.80	0.19	1.17	2.44

https://doi.org/10.1021/acsomega.3c10247
ACS Omega 2024, 9, 15357−15371

percentage of isolated pore volume for each type of pore. The connected pores can also be divided into three types: D, E, and F. Of these, the pore volume of type D is less than 10^6 μm^3. Type E has a pore volume of 10^6–10^7 μm^3, and type F has a pore volume greater than 10^7 μm^3. Table 3 shows the percentage of connected pore volume of each type of pore. Irrespective of whether the pores are isolated or connected, the large-volume pores occupy dominant positions in the pore system. These coal samples, therefore, not only store coalbed methane well but also contain good migration channels to release the coalbed methane. The connected pores are the main factor affecting the connectivity of the coal samples; therefore, the volume proportion of connected pores should be assessed to evaluate the coal sample connectivity. Of the four types of samples, the PY samples occupy a small proportion of the connected pore volume and show poor connectivity.

Table 3. Volume Percentage of Connected Pores

sample number	percentage of total connected pore volume (%)	percentage of pore volume (%)		
		D	E	F
LZ	4.32	0.01	0.88	3.43
RL	5.53	0.11	2.41	3.01
PY	3.39	0.13	1.76	1.50
QD	8.10	0.21	5.24	2.65

3.3. Characterization and Analysis of the Equivalent Pore Network Model. *3.3.1. Equivalent Pore Network Model Extraction.* The equivalent pore network is a model that provides a simplified model of the complex connected pore structure in coal rock. The connected pore structure has been reconstructed by CT and the pore network model (PNM) using AVIZO software, after which an equivalent pore network model, the ball-and-stick model, was developed. This model uses the principle of maximum sphere algorithm,[40] where several spheres occupy the pore fracture space in the porous media, and where the pore fractures and throats have been identified. A sphere is called a maximum sphere if it fills the pore fracture space and is not fully contained by other spheres. A local maximum sphere is then defined as a pore body, and the link between the largest spheres is called the throat, which is used to build the equivalent pore network model (Figure 9).

3.3.2. Parameter Analysis of the Equivalent Pore Network Model. The structure of connected pores can be used to extract the equivalent pore network model, while the AVIZO software can quantitatively count some of the characteristic parameters. The number of LZ-connected pores is 395 and the number of throats is 1166. The number of connected pores in the RL samples was 836 and the number of throats was 3363. PY has 582 connected pores and 1262 throats, while QD has 1491 connected pores and 4827 throats. Table 4 lists some additional parameters.

The coordination number, throat radius, and throat length have a significant effect on the connectivity of the coal samples and must be statistically analyzed. Statistical analyses show that the coordination numbers of the LZ, RL, PY, and QD coal samples are distributed within 1–20, indicating that more throats connect the pores and that the pores have good connectivity. The dominant coordination numbers of the sample include LZ = 4–6, RL = 4–9, PY = 3–6, and QD = 2–8 (Figure 10), indicating that all four samples have good connectivity based on the angle of the pores. Since the pores with coordination number 1 are dead-end pores, samples with a large number of these pores will reduce the connectivity of the sample. Sample PY has a large number of dead-end pores, and therefore, the connectivity of sample PY is poor compared to the other samples. The equivalent pore network model (Figure 9) shows that the connected pores of samples LZ and QD are better distributed in space, while sample LZ is the best. The average coordination numbers of samples LZ and QD are better than the other samples, indicating good connectivity, while the changes in the coordination number of the samples in Figure 10 reflect the quantitative equilibrium between the pores and the throats. Samples with lower variation in the coordination number show better balance. The variation in the coordination numbers of samples LZ and QD is low and the pores in these samples are better connected. However, the variation in the coordination

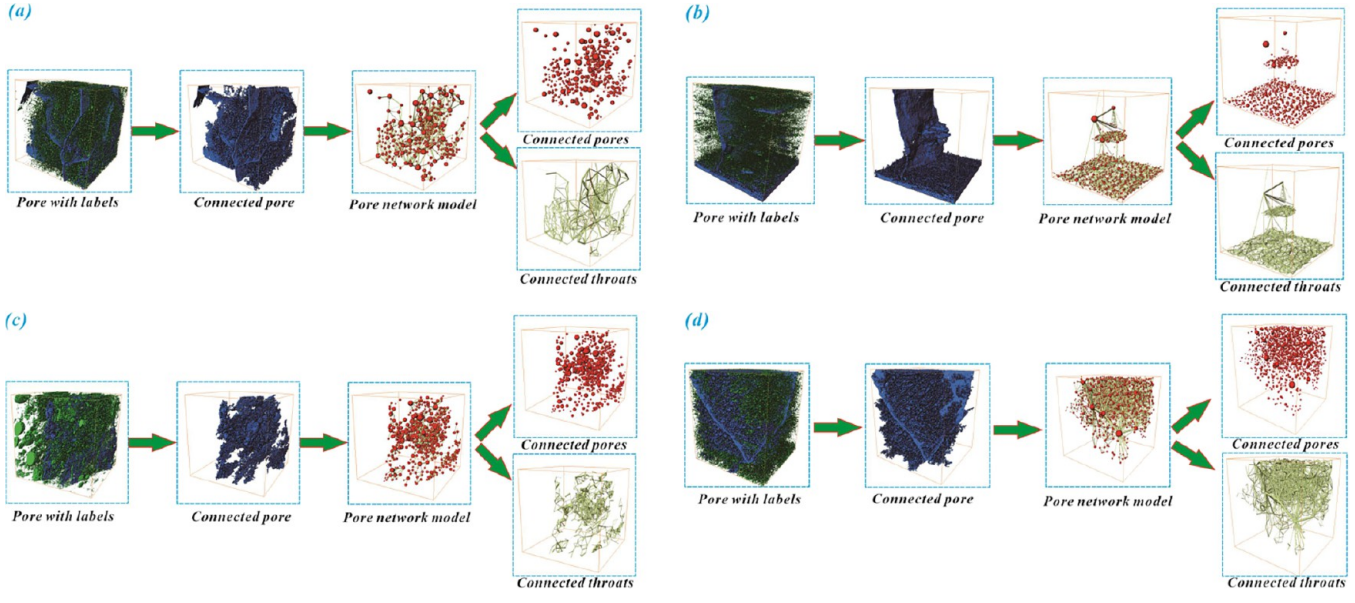

Figure 9. Extraction flowchart of the equivalent pore and fissure network model: (a) LZ sample; (b) RL sample; (c) PY sample; (d) QD sample.

https://doi.org/10.1021/acsomega.3c10247
ACS Omega 2024, 9, 15357−15371

Table 4. Quantitative Parameter Statistics of the Connected Coal Sample Pore Fissure Network Model

sample		pore volume (μm^3)	pore EqRadius (μm)	throat EqRadius (μm)	throat length (μm)	coordination number
LZ	max	2.67×10^8	399.41	204.49	2790.38	34
	min	5.26×10^4	23.25	2.30	33.52	1
	Average	5.67×10^6	93.56	45.08	283.94	8.05
RL	max	1.61×10^8	337.38	170.70	1984.57	23
	min	3.05×10^5	41.76	3.34	74.92	1
	average	1.37×10^7	128.67	42.39	491.54	5.90
PY	max	7.71×10^7	264.00	223.99	766.29	20
	min	0.76×10^5	26.26	2.42	50.31	1
	average	4.01×10^6	84.78	32.65	272.52	4.34
QD	max	1.61×10^8	337.78	132.70	1689.47	79
	min	1.31×10^5	31.50	2.25	49.34	1
	average	0.41×10^8	88.46	26.59	333.88	6.47

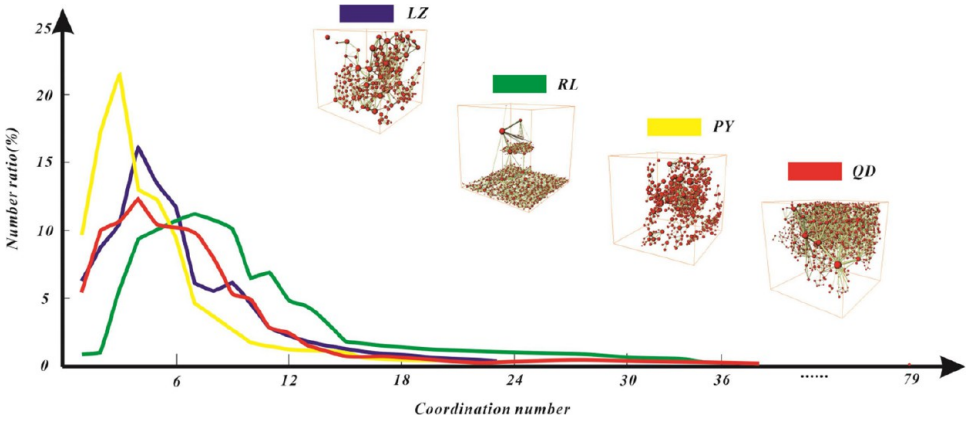

Figure 10. Sample coordination number proportions.

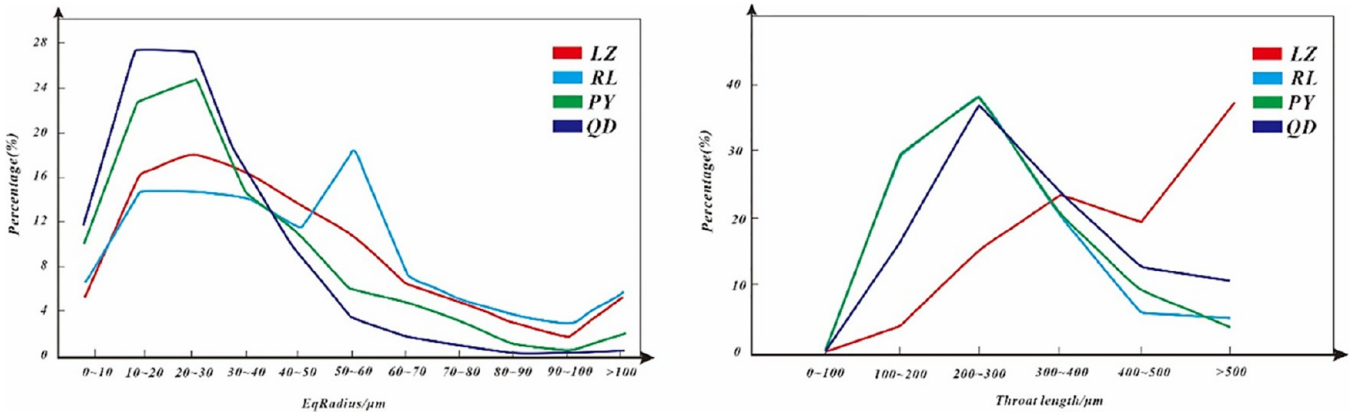

Figure 11. Diagram of throat parameters.

numbers of sample PY is large, and this sample has poor balance and pore connectivity.

An analysis of the throat parameters, based on the above coordination numbers and the overall perspective, indicates that the connectivity between samples LZ and QD was good, while the connectivity between samples RL and PY was poor. Using these conditions, samples LZ and QD were grouped, and samples RL and PY were grouped. The connectivity of the samples in different places was then further analyzed. Half of the proportion of throat parameters was selected based on statistical analyses. Based on Figure11, the number of throats in the LZ sample with a throat radius of 10−60 μm accounted for 74.5%, while the proportion of each interval was more balanced. The number of throats in the QD samples with a throat radius of 10−40 μm accounted for 71.4%, and the throat number of QD samples with a throat radius of 10−40 μm accounted for a range of 10 μm. The number of throats in 10−30 μm was more prominent. The LZ samples had a throat length of 200−500 μm and the throat number of QD samples accounted for 58.5%, while the QD samples had a throat length of 200−400 μm and a throat number of 59.8%. Considering the average analysis of the throat parameters of the LZ and QD samples, the connectivity of the LZ samples is better than that of the QD samples. Similarly, the RL samples showed better connectivity than the PY samples.

3.3.3. Permeability Analysis Based on the Pore Network Model. The connectivity difference of the coal samples will affect their permeability. Understanding the permeability of coal samples can, therefore, enhance the connectivity analysis of coal

https://doi.org/10.1021/acsomega.3c10247
ACS Omega 2024, 9, 15357−15371

samples. The PNM model of the AVIZO software can experimentally simulate the permeability of coal samples in different directions and obtain certain parameters by using the algorithm carried out by the software itself (Table 5). Throats, as

Table 5. Absolute Permeability of the Connected Pore Structures in Different Directions

	absolute permeability (μm^2)		
sample	*X* direction	*Y* direction	*Z* direction
LZ	0.6742	24.9986	14.5732
RL	22.8194	0.0552	0.3381
PY	0.2051	0.0900	−8.3358
QD	0.2534	7.5672	0.0253

the connection channels between the pores, not only affect the permeability of the coal reservoir but also directly affect fluid migration in the coal reservoir. The AVIZO software can intuitively observe changes in the fluid flow (Figure 12). In Figure 12, blue represents small flows, and red represents large flows in the *X*, *Y*, and *Z* directions of the respective coal samples. The input pressure is set to 0.13 MPa, and the output pressure is set to 0.1 MPa. The fluid viscosity is set to 0.001 Pa s.

According to the results of permeability simulation experiments, it can be seen that the fluid seepage of the LZ and QD samples is better than that of the other two samples in terms of spatial distribution, and at the same time, it reflects better connectivity and is consistent with the results of the previous analysis. Figure 12 shows that compared to the other samples, the structure between the throats of the LZ samples is relatively simple, with a low degree of bending, and therefore, the fluid permeability is relatively good. The permeability of the LZ sample is better than that of the other samples, while the permeability of the LZ sample in the *Y*-axis direction not only is better than that of the other samples but also performs better compared to the other samples (Table 5). At the same time, it can be seen that the permeability of the RL sample in the *X*-axis direction is excellent.

4. DISCUSSION

4.1. Selection and Application of the REV before Pore Structure Analysis. The REV in this study was selected based on the central part of the slice and the central part of the coal sample (Figure 13). After analyses, cubes with a REV size of 500 × 500 × 500 voxels were selected for further analyses of the LZ, RL, PY, and QD coal samples (Figure 14).

First, the selection of the cube size was based on the central part of the 2D slice. Cube extraction was then carried out based on the distribution of the continuous slices. The final size of the REV was determined according to the changes in the porosities of the extracted coal samples with different sizes.

When the cube size of the sample LZ was smaller than the voxels of part III (500 × 500 × 500), the changes in the porosity of part I and part II and the REV were rather disordered. When the cube size of the LZ sample is located in part III, the changes in the porosity were relatively stable, and the porosity only began to fluctuate a little when it reached part IV. The stable voxel cube size of 500 × 500 × 500 was therefore selected for the study, and the corresponding operations were carried out in the same way on other samples. When the voxel cube size of other samples was larger than 500 × 500 × 500, the hole fissure tended to be stable, and the size of a 500 × 500 × 500 cube was also selected for the study.

4.2. Connectivity of the Coal Samples Based on Connected Pore Classification and Quantitative Analysis. The pores in coal can be divided into connected and isolated pores. The connected pores provide the storage and migration pathways for coalbed methane. A better understanding of the connected pores helps us to understand coal reservoir connectivity. Whether methane is directly mined or extracted via gas injection mining (CO_2-ECBM), the connected pores in the coal reservoirs will directly affect the economic viability of the coalbed methane. A good understanding of the connected pores of coal samples in reservoirs is therefore required.

Connected pores can be further divided into fractures and effectively connected pores, but there is no definite difference between fractures and pores at present. These two features were therefore studied together in this study, while the distribution relationship between them was also analyzed (Figure 15).

Figure 15a generally shows a large volume of connected pores, which represents the main migration channel of fluid in coal and which affects coal seam gas exploitation. Figure 15b indicates the storage sites and migration channels for the coal seam gas in the coal reservoirs but mainly indicates storage. The distribution of connected pores in Figure 15c is ideal for the exploration and development of coalbed gas. The pores indicated in Figure 15c have a good methane storage potential and also show good migration channels for the extraction of coalbed methane. These channels not only make the coal seam structure more stable but also allow for overall communication throughout the coal seam. Proper pores and migration channels are very important for the development of coalbed methane and the potential evaluation of coalbed methane resources.

The connected pores of the coal samples have been divided based on their pore equivalent radius. Pores with a radius of 10−30 μm occupy a relatively dominant position in the four coal samples, indicating that the pores in this range frequently occur in the low-permeability coal seams of Huainan−Huaibei (Figure 16). The main pore type of the LZ samples is the connected pore with a pore size of 10−60 μm. The connected pore diameter of the RL samples is relatively average in each aperture range while the connected pore radius for the PY and QD coal samples ranges from 10 to 40 μm. Based on the previous analysis results, the connected pores with pore sizes ranging from 10 to 40 μm allow for a better-connected pore system in the coal samples, and the coal samples with a pore distribution in this range show better pore connectivity.

4.3. Role of the Coordination Number on the Connectivity of the Coal Reservoir Pore Structure. Based on previous analyses, the basic units of the equivalent pore network model include the reservoir pores and throats that act as migration channels between the pores. The black circle in Figure 17, represents the pore; the red column represents the throat; and the dashed blue line represents the fluid movement at the sample site. P_{in} is the inlet pressure, P_{out} is the outlet pressure, and the blue arrow shows the direction of the fluid movement.

Figure 17a,b shows that isolated pores have connected pores inside the coal sample and that the fluid activity area cannot penetrate the coal rock; therefore, there is no connectivity. Figure 17c shows a connected pore that can communicate with the outside world. Fluid can pass through the coal sample through the internal channel with good connectivity.

Figure 17d−f shows the influence of throat and pore quantity equilibrium on connectivity. The number of pores and throats is

https://doi.org/10.1021/acsomega.3c10247
ACS Omega 2024, 9, 15357−15371

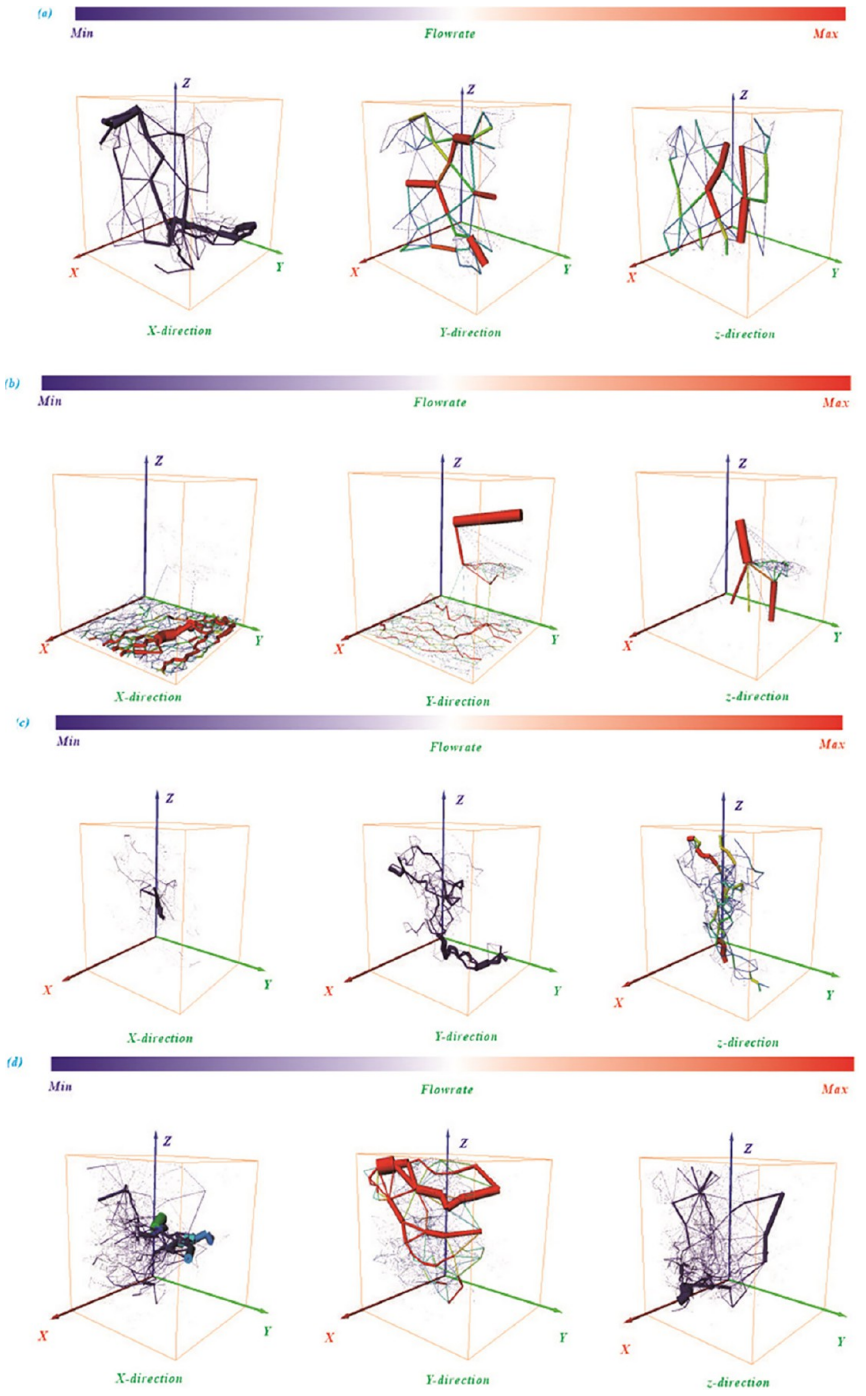

Figure 12. PNM-based visualization of 3D directional gas migration paths: (a) LZ sample; (b) RL sample; (c) PY sample; and (d) QD sample.

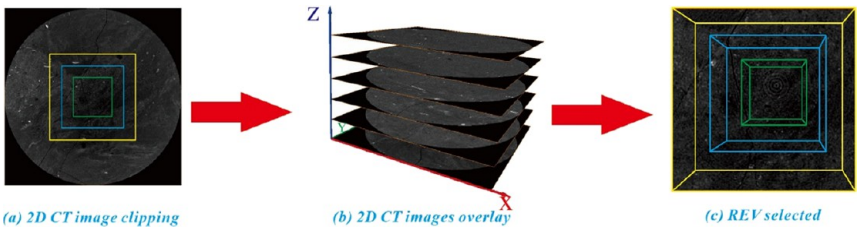

Figure 13. Representative elementary volume stability analysis. (a) 2D CT image clipping. (b) 2D CT image overlay. (c) REV selected.

poorly balanced, and fluid enters from the left, while its final active area is limited to the right, indicating poor connectivity (Figure 17d). As can be seen from Figure 17e, the number of pores and throats is generally balanced, and fluid can easily flow

https://doi.org/10.1021/acsomega.3c10247
ACS Omega 2024, 9, 15357−15371

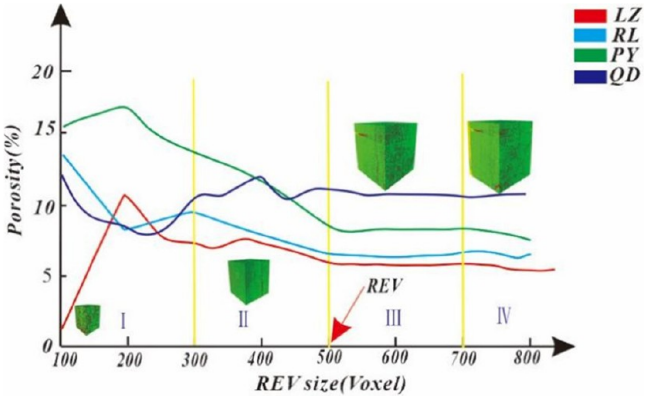

Figure 14. Representative Elementary Volume stability analysis.

along the channel in a certain direction, but it cannot move in the entire region of the coal sample. Figure 17f shows that the quantity balance between the pores and the throat is good and that the fluid that enters the sample from the left side can eventually move through the whole sample, indicating that the sample has good connectivity.

The above method has been used to evaluate the connectivity of the LZ, RL, PY, and QD samples. The constructed three-dimensional model that was based on statistical data, combined with the equivalent pore fracture network model, shows that the LZ sample performs better than the other three samples in terms of the local angle and the overall angle of the sample. This means that the LZ sample has an ideal connectivity.

4.4. Permeability Analysis Based on the Combination of Different Types of Throats. The permeability of the coal reservoir directly reflects the quality of the coal sample connectivity and helps in the analysis of the coal seam connectivity. The AVIZO software can extract the connected pore structure and build an equivalent pore network model based on this structure. The AVIZO model allows for visual observation of the distribution, migration, and flow changes of the fluids in the connected pores based on color changes. Red indicates a high flow rate, and blue indicates a low flow rate. In the equivalent pore network model, the black circles represent the pores, and columns of different colors and sizes represent the different flow rates of the throats (Figure 18). Light blue is 0, which is greater than light blue, plus 1 for every step up and less than light blue, minus 1 for every step down.

The larger the equivalent radius of the throat, the better the permeability to the coal sample and the better the overall condition than the possible result of the arrangement and combination of the various types of throats (Figure 18d–f). Figure 18a–c shows that the smaller the equivalent radius of the throat, the worse the permeability of the coal sample. The overall permeability of the coal samples with a large equivalent radius connected to throat samples with a small equivalent radius is better than that of coal samples with the opposite equivalent radius (Figure 18g–i,j–l).

When considering only the thickness of the coal sample throat, the permeability of the coal sample with the throat distribution in Figure 18e is better than that of the other samples, while Figure 18c is the worst. When considering the collocation of the throat thickness, the distribution of the throats in Figure 18k is the best, while the distribution of the throats in Figure 18i is the worst.

Even though permeability analyses help in the study of pore connectivity, there are certain limitations to this study. Real-world permeability analyses are complicated by changes in the pore structure, which is influenced by changes in reservoir stress during coal seam gas exploitation.

4.5. Evolution of the Connected Pore Structure in CO_2-ECBM Time. The connected pores can be further divided into cracks and effectively connected pores. This allows for analyses of the structural evolution, connectivity, and permeability advantages and shortcomings of connected pores in CO_2-ECBM (Figure 19). In Figure 19, gray represents the coal matrix, yellow is the effective connecting hole, white represents the fracture, A is the gas injection well, and B is the production well.

Near the gas injection area, the pore structure changes of the coal reservoirs are mainly influenced by the effective reservoir stress and competitive adsorption of CH_4 and CO_2 (Figure 19). CO_2 injection can reduce the effective stress of the coal reservoirs and improve the fracture porosity in the vicinity of the gas injection wells, which improves the connectivity and permeability. However, at the same time, injected CO_2 will competitively adsorb with CH_4. Since the coal matrix will preferentially adsorb CO_2, large volumes of CO_2 will be adsorbed, which will cause a great expansion of the coal matrix. This expansion will reduce the effective porosity of the coal matrix, which reduces the connectivity and permeability of the coal sample. Simultaneously, the expansion of the coal matrix affects the connected pore structure of the reservoir to a larger degree than the effective stress of the reservoir. Over time, the coal matrix will develop poorer connectivity, and the permeability in areas close to the gas injection well will decrease.

Near the production area, where CO_2 does not reach, the coal reservoir permeability is mainly influenced by the effective reservoir stress and the matrix contraction caused by CH_4 desorption. During the initial stages of coalbed methane extraction, the boundary pressure relief of the production wells increases the effective stress on fractures in the reservoir. This reduces the fracture porosity, which further reduces the connectivity and permeability. The boundary pressure relief of the production wells also causes the desorption of CH_4, which causes a contraction of the coal matrix and improves the effective porosity. However, the migration of free CH_4 in the fracture will increase the pressure in the fracture and delay the reduction of the fracture. Over time, the influence of CH_4 desorption on the porosity of the coal reservoir becomes more dominant. The

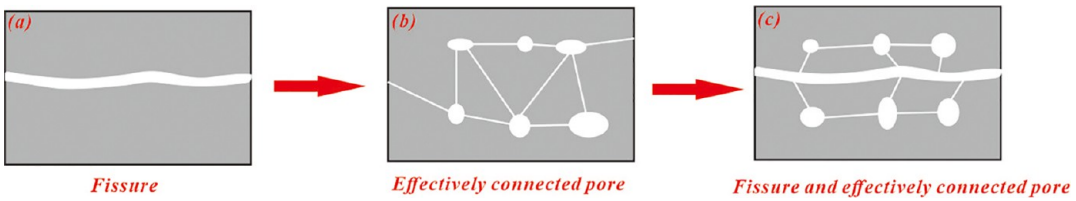

Figure 15. Connected pore analysis. (a) Fissure; (b) effectively connected pore; (c) fissure and effectively connected pore.

https://doi.org/10.1021/acsomega.3c10247
ACS Omega 2024, 9, 15357−15371

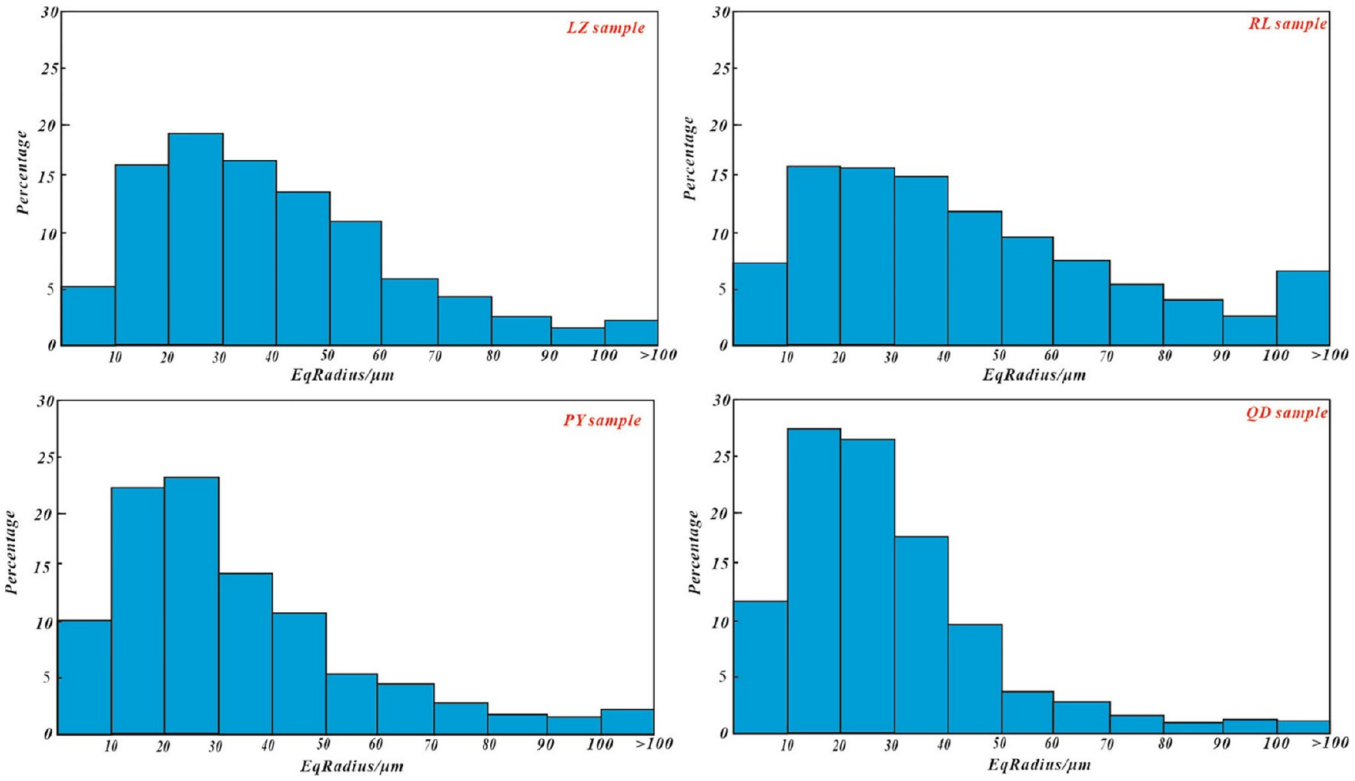

Figure 16. Percentage of the equivalent pore radius.

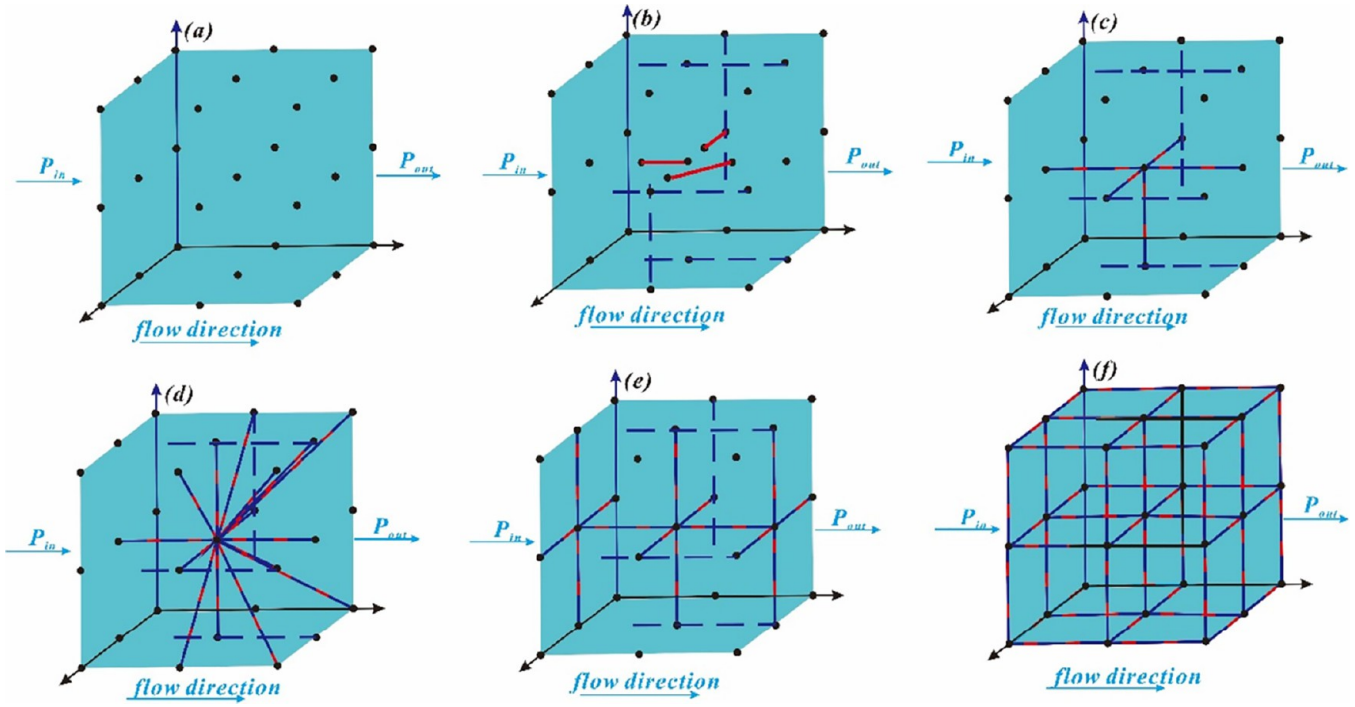

Figure 17. Effect of coordination number on the connectivity of the pores. (a−c) Difference in coordination number; (d−f) difference in the balance of the number of pores and throats.

combined effect of CH_4 desorption and the effective stress improves the fracture porosity and effectively connects the porosity of the coal reservoir. This means that when the CO_2 reaches the production zone, the changes in its connected pore structure are consistent with those of the gas injection zone.

5. CONCLUSIONS

This study constructed a 3D model and an equivalent pore network model of coal samples from the Huainan−Huaibei coalfield. The pore structure of coal reservoirs is analyzed from a multidimensional perspective and from a global to a local perspective. Based on the three-dimensional visualization of the

https://doi.org/10.1021/acsomega.3c10247
ACS Omega 2024, 9, 15357−15371

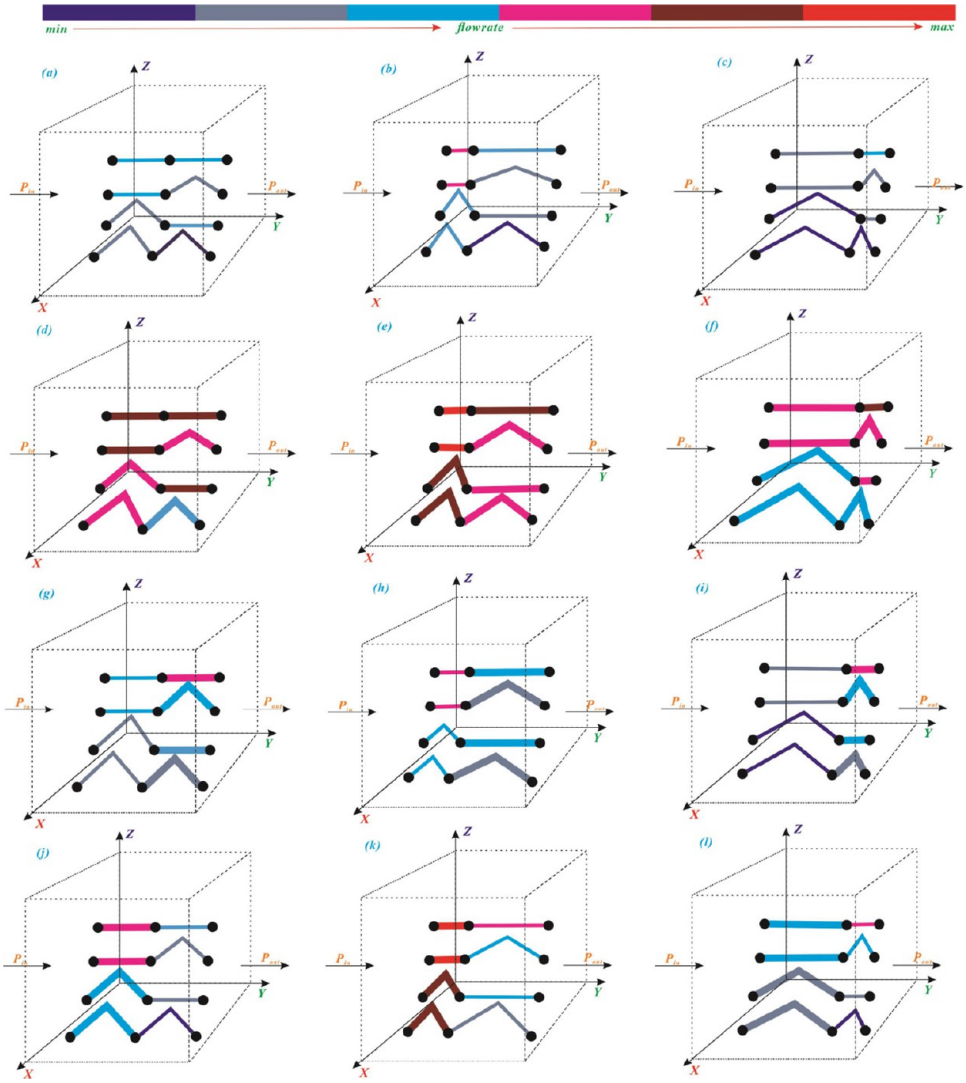

Figure 18. Analysis of the throat distribution. (a−c) Collocation between the long and short types of fine throats; (d−f) Collocation between the long and short types of coarse throats; (g−l) Collocation between long and short types of fine and coarse throats.

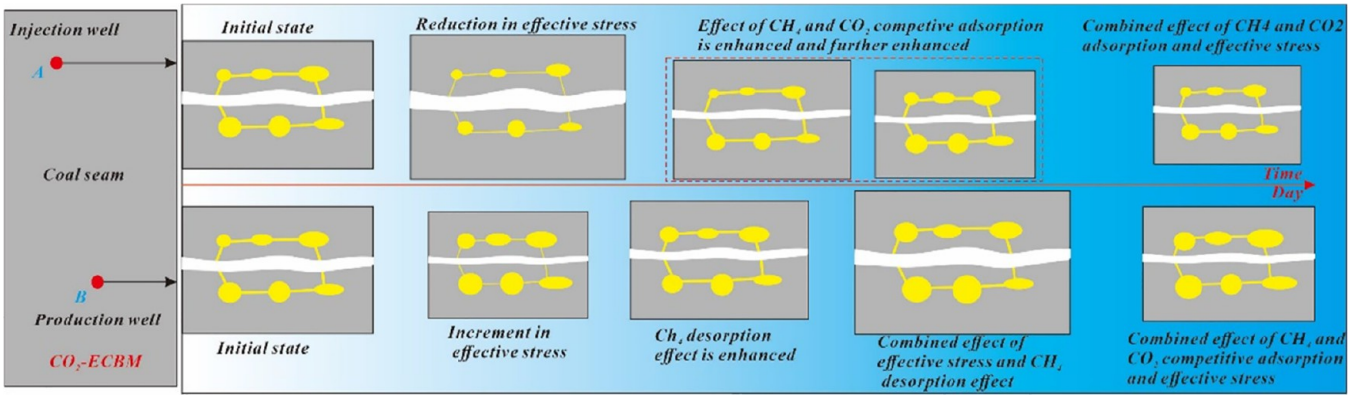

Figure 19. Connected pore structure changes during the CO_2-ECBM process.

pore structure, the equivalent pore network model, and the characteristic parameters of the pore structure, the comprehensive analysis of pore structure connectivity and permeability of the coal reservoir is realized. The main conclusions are as follows:

1. Quantitative analysis shows that the porosity and representative elementary volumes of the size (500 × 500 × 500) are the most suitable. Quantitative analysis of the pore and fracture structure parameters shows that the surface porosity of the two-dimensional slice of the Ren Lou sample has a value close to 0 in the *Y*-axis direction,

https://doi.org/10.1021/acsomega.3c10247
ACS Omega 2024, 9, 15357−15371

indicating poor connectivity compared to other samples. Second, statistical analyses of the volume parameters of the connected and isolated pores show that large-volume connected pores dominate their pore systems, while connected pores with a radius of 10−30 μm dominate in the coal samples.

2. The coordination numbers of the samples ranged from 1−20. Based on the equivalent network model and the three-dimensional visualization of the pore structure, the connectivity of the coal samples can be analyzed. The connectivity of the LZ samples was better than that of the other samples both from the perspective of locality and the perspective of the coal samples as a whole. The connectivity of the RL and PY samples was relatively poor, while the connectivity of the PY sample was the worst.
3. Based on the equivalence network model, it is possible to simulate the experiment of fluid permeability in different directions of the same sample. It showed that the Liuzhuang sample is more permeable than the other samples, and the permeability was best in the *Y*-axis direction. For any combination of different types of throats, the shorter the throat, the greater the equivalent radius, and the better the permeability.
4. After further dividing the connected pores, the evolution of the connected pore structure during CO_2-ECBM could be determined. Near the gas injection area, the connectivity and permeability decreased over time close to the gas injection well. Near the production area, where the CO_2 did not reach, the fracture porosity and effectively connected porosity of the coal reservoir increased over time. Where the CO_2 reached the production area, the changes in its connected pore structure were consistent with those in the gas injection area.

AUTHOR INFORMATION

Corresponding Authors

Huihuang Fang − *School of Earth and Environment and State Key Laboratory of Mining Response and Disaster Prevention and Control in Deep Coal Mines, Anhui University of Science and Technology, Huainan, Anhui 232001, China; Department of Geological Sciences, University of Saskatchewan, Saskatoon, SK S7N 5E2, Canada;* orcid.org/0000-0002-1139-5525; Email: huihuangfang@aust.edu.cn

Shuxun Sang − *Carbon Neutrality Institute and Jiangsu Key Laboratory of Coal-Based Greenhouse Gas Control and Utilization, China University of Mining and Technology, Xuzhou 221008, China; School of Resources and Geosciences, China University of Mining and Technology, Xuzhou 221116, China*; Email: shxsang@cumt.edu.cn

Authors

Zhangfei Wang − *School of Earth and Environment and State Key Laboratory of Mining Response and Disaster Prevention and Control in Deep Coal Mines, Anhui University of Science and Technology, Huainan, Anhui 232001, China*

Jinran Guo − *School of Earth and Environment and State Key Laboratory of Mining Response and Disaster Prevention and Control in Deep Coal Mines, Anhui University of Science and Technology, Huainan, Anhui 232001, China*

Shua Yu − *School of Earth and Environment and State Key Laboratory of Mining Response and Disaster Prevention and Control in Deep Coal Mines, Anhui University of Science and Technology, Huainan, Anhui 232001, China*

Huihu Liu − *School of Earth and Environment and State Key Laboratory of Mining Response and Disaster Prevention and Control in Deep Coal Mines, Anhui University of Science and Technology, Huainan, Anhui 232001, China;* orcid.org/0000-0002-6703-0357

Hongjie Xu − *School of Earth and Environment and State Key Laboratory of Mining Response and Disaster Prevention and Control in Deep Coal Mines, Anhui University of Science and Technology, Huainan, Anhui 232001, China;* orcid.org/0000-0003-0143-3804

Complete contact information is available at: https://pubs.acs.org/10.1021/acsomega.3c10247

Notes

The authors declare no competing financial interest.

ACKNOWLEDGMENTS

We would like to express our gratitude to the anonymous reviewers for offering their constructive suggestions and comments which improved this manuscript in many aspects. This work was financially supported by the Anhui Provincial Key Research and Development Project (2023z04020001), the Anhui Provincial Natural Science Foundation (2308085Y30), the Natural Science Research Project of Anhui Educational Committee (2023AH040154), the National Natural Science Foundation of China (No. 42102217; 42277483), and the University Synergy Innovation Program of Anhui Province (No. GXXT-2021-018).

REFERENCES

(1) Yao, Y.; Liu, D.; Cai, Y.; et al. Advanced characterization of pores and fractures in coals by nuclear magnetic resonance and X-ray computed tomography. *Sci. China Earth Sci.* **2010**, *53* (06), 854−862.

(2) Wang, H.; Chen, S.; Zhang, S. Study on fracture characteristics in coal and shale for coal-measure gas reservoir based on 3D CT reconstruction and fractal features. *Front. Earth Sci.* **2023**, *17*, 514−526.

(3) Ni, H.; Liu, J.; Chen, T.; Chen, S.; et al. Coal permeability prediction method based on the microscopic pore-fracture dual-porosity structure. *J. Petrol. Sci. Eng.* **2022**, *211*, 110107.

(4) Wang, G.; Qin, X.; Zhou, J.; et al. Simulation of coal microstructure characteristics under temperature-pressure coupling based on micro-computer tomography. *Journal of Natural Gas Science and Engineering* **2021**, *91*, 103906.

(5) Liang, W.; Wang, J.; Sang, S.; et al. The influence of closed pores and stacked coal grains on gas transport in CO_2 injection enhanced CH_4 recovery process. *J. Petrol. Sci. Eng.* **2022**, *212*, 110303.

(6) Fang, H.; Sang, S.; Du, Y.; et al. Visualization characterization of minerals touched by interconnected pores and fractures and its demineralization effect on coal permeability during CO_2-ECBM process based on X-ray CT data. *J. Nat. Gas Sci. Eng.* **2021**, *95*, 104213.

(7) Sok, R. M.; Knackstedt, M. A.; Sheppard, A. P.; et al. Direct and stochastic generation of network models from tomographic images; effect of topology on residual saturations. *Transport in porous media* **2002**, *46*, 345−371.

(8) Lindquist, W. B.; Venkatarangan, A.; Dunsmuir, J.; et al. Pore and throat size distributions measured from synchrotron X-ray tomographic images of Fontainebleau sandstones. *Journal of Geophysical Research: Solid Earth* **2000**, *105* (B9), 21509−21527.

(9) Chen, X.; Ma, R.; Wu, J.; et al. Fractal Analysis of Coal Pore Structure Based on Computed Tomography and Fluid Intrusions. *Fractal and Fractional* **2023**, *7* (6), 439.

(10) Miao, Z.; Xuehai, F.; Chaochao, D.; et al. Influencing factor analysis of the coal matrix compressibility of middle-high rank coals. *Journal of Natural Gas Science and Engineering* **2020**, *81*, 103462.
(11) Wu, H.; Yao, Y.; Emmanuel, S. Interactive Machine Learning Improves Accuracy of Coal Porosity Segmentation in Focused Ion Beam−Scanning Electron Microscopy Images. *Energy Fuels* **2023**, *37* (14), 10466−10473.
(12) Li, Y.; Yang, J.; Pan, Z.; et al. Nanoscale pore structure and mechanical property analysis of coal: An insight combining AFM and SEM images. *Fuel* **2020**, *260*, 116352.
(13) Zhang, G.; Ranjith, P. G.; Fu, X.; et al. Pore-fracture alteration of different rank coals: Implications for CO2 sequestration in coal. *Fuel* **2021**, *289*, 119801.
(14) Li, Q.; Ma, D.; Zhang, Y.; et al. Insights into controlling factors of pore structure and hydraulic properties of broken rock mass in a geothermal reservoir. *Lithosphere* **2021**, *2021* (Special 5), No. 3887832, DOI: 10.2113/2022/3887832.
(15) Wang, Z.; Qin, Y.; Shen, J.; et al. A novel permeability prediction model for coal based on dynamic transformation of pores in multiple scales. *Energy* **2022**, *257*, 124710.
(16) Li, Z.; Zhang, G. Fracture segmentation method based on contour evolution and gradient direction consistency in sequence of coal rock CT images. *Math. Probl. Eng.* **2019**, *2019*, No. 2980747, DOI: 10.1155/2019/2980747.
(17) Fu, X.; Dai, J.; Feng, J. Prediction of tectonic fractures in coal reservoirs using geomechanical method. *Geosciences Journal* **2018**, *22*, 589−608.
(18) Fang, H. H.; Wang, Z. F.; Sang, S. X.; et al. Numerical analysis of matrix swelling and its effect on microstructure of digital coal and its associated permeability during CO_2-ECBM process based on X-ray CT data. *Petroleum Science* **2023**, *20* (1), 87−101.
(19) Hao, J.; Shu, L.; Huo, Z. Quantitative characterization of pore-fracture structure of medium and high-rank coal based on micro-CT technology. *Int. J. Coal Prep. Util.* **2024**, *44*, 358−375.
(20) Wang, G.; Qin, X.; Shen, J.; et al. Quantitative analysis of microscopic structure and gas seepage characteristics of low-rank coal based on CT three-dimensional reconstruction of CT images and fractal theory. *Fuel* **2019**, *256*, 115900.
(21) Wang, H.; Chen, S.; Li, X.; et al. Quantitative characterization of fracture in the coal of Shanxi and Taiyuan formations based on an image processing method and multifractal theory. *Energy Fuels* **2021**, *35* (15), 12019−12029.
(22) Li, Y.; Jiang, Y.; Zhang, B. Investigation on the pore characteristics of coal specimens with bursting proneness. *Sci. Rep.* **2019**, *9* (1), No. 16518.
(23) Jia, P.; Nadimi, S.; Jia, J. Quantitative micro mechanical and pore structural characterisation of coal before and after freezing. *Fuel* **2022**, *316*, 123421.
(24) Wang, G.; Shen, J.; Liu, S.; et al. Three-dimensional modeling and analysis of macro-pore structure of coal using combined X-ray CT imaging and fractal theory. *International Journal of Rock Mechanics and Mining Sciences* **2019**, *123*, 104082.
(25) Wu, Y.; Wang, D.; Wang, L.; et al. An analysis of the meso-structural damage evolution of coal using X-ray CT and a gray-scale level co-occurrence matrix method. *International Journal of Rock Mechanics and Mining Sciences* **2022**, *152*, 105062.
(26) Hou, C.; Jiang, B.; Li, M.; et al. Micro-deformation and fracture evolution of in-situ coal affected by temperature, confining pressure, and differential stress. *Journal of Natural Gas Science and Engineering* **2022**, *100*, 104455.
(27) Wu, Y.; Wang, D.; Pang, X. Study on the Fracture Evolution Law of Coal Based on Image Retrieval Method and X-Ray Computed Tomography. *Geofluids* **2022**, *2022*, No. 6234708, DOI: 10.1155/2022/6234708.
(28) Jing, Y.; Armstrong, R. T.; Mostaghimi, P. Image-based fracture pipe network modelling for prediction of coal permeability. *Fuel* **2020**, *270*, 117447.
(29) Wu, H.; Yao, Y.; Zhou, Y.; et al. Analyses of representative elementary volume for coal using X-ray μ-CT and FIB-SEM and its application in permeability predication model. *Fuel* **2019**, *254*, 115563.
(30) Wei, M. Y.; Liu, J.; Liu, Y. K.; et al. Effect of adsorption-induced matrix swelling on coal permeability evolution of micro-fracture with the real geometry. *Petroleum Science* **2021**, *18* (4), 1143−1152.
(31) Prodanović, M.; Lindquist, W. B.; Seright, R. S. 3D image-based characterization of fluid displacement in a Berea core. *Advances in Water Resources* **2007**, *30* (2), 214−226.
(32) Vogel, H. J.; Roth, K. Quantitative morphology and network representation of soil pore structure. *Advances in water resources* **2001**, *24* (3−4), 233−242.
(33) Fang, H.; Xu, H.; Sang, S. 3D reconstruction of coal pore network and its application in CO 2-ECBM process simulation at laboratory scale. *Front. Earth Sci.* **2022**, *16*, 523−539.
(34) Da Wang, Y.; Shabaninejad, M.; Armstrong, R. T. Deep neural networks for improving physical accuracy of 2D and 3D multi-mineral segmentation of rock micro-CT images. *Appl. Soft Comput.* **2021**, *104*, No. 107185.
(35) Liu, W.; Han, D.; Wang, G.; et al. Representative elementary volume evaluation of coal microstructure based on CT 3D reconstruction. *Fuel* **2023**, *336*, 126965.
(36) Liu, P.; Nie, B.; Zhao, Z.; et al. Permeability of micro-scale structure in coal: Insights from μ-CT image and pore network modelling. *Gas Science and Engineering* **2023**, *111*, 204931.
(37) Fu, Yu; Xin, Chen; Zhongliang, Feng Characteristics of coal-rock fractures based on CT scanning and its influence on failure modes. *J. China Coal Soc.* **2020**, *45* (2), 568−578.
(38) Zhao, Y.; Sun, Y.; Liu, S.; et al. Pore structure characterization of coal by synchrotron radiation nano-CT. *Fuel* **2018**, *215*, 102−110.
(39) Shi, X.; Pan, J.; Pang, L.; et al. 3D microfracture network and seepage characteristics of low-volatility bituminous coal based on nano-CT. *Journal of Natural Gas Science and Engineering* **2020**, *83*, 103556.
(40) Silin, D.; Patzek, T. Pore space morphology analysis using maximal inscribed spheres. *Physica A: Statistical mechanics and its applications* **2006**, *371* (2), 336−360.

https://doi.org/10.1021/acsomega.3c10247
ACS Omega 2024, 9, 15357−15371